The endoplasmic reticulum-mitochondria interface is perturbed in PARK2 knockout mice and patients with PARK2 mutations

Clément A. Gautier, Zoi Erpapazoglou, François Mouton-Liger, Marie Paule Muriel, Florence Cormier, Stéphanie Bigou, Sophie Duffaure, Mathilde Girard, Benjamin Foret, Angelo Iannielli, et al.

The endoplasmic reticulum-mitochondria interface is perturbed in *PARK2* knockout mice and patients with *PARK2* mutations

Clément A. Gautier[1-4,#,†], Zoi Erpapazoglou[1-4,†], François Mouton-Liger[1-4], Marie Paule Muriel[1-4], Florence Cormier[1-4], Stéphanie Bigou[1-4], Sophie Duffaure[1-4], Mathilde Girard[5], Benjamin Foret[5], Angelo Iannielli[6,7], Vania Broccoli[6,7], Carine Dalle[1-4], Delphine Bohl[1-4], Patrick P. Michel[1-4], Jean-Christophe Corvol[1-4,8], Alexis Brice[1-4], and Olga Corti[1-4,*].

[1]Inserm, U1127, F-75013, Paris, France, [2]CNRS, UMR 7225, F-75013, Paris, France, [3]Sorbonne Universités, UPMC Univ Paris 06, UMR S 1127, F-75013, Paris, France, [4]Institut du Cerveau et de la Moelle épinière, ICM, F-75013, Paris, France, [5]CECS, I-Stem, AFM, Institute of Stem Cell Therapy and Exploration of Monogenic Diseases, 91030, Evry cedex, France, [6]Division of Neuroscience, San Raffaele Scientific Institute, 20132 Milan, Italy, [7]National Research Council (CNR), Institute of Neuroscience, Milan, Italy, [8]Assistance-publique Hôpitaux de Paris, Inserm, CIC-1422, Department of Neurology, Hôpital Pitié-Salpêtrière, F-75013, Paris, France

[*]To whom correspondence should be addressed at: Institut du Cerveau et de la Moelle épinière-Hôpital Pitié-Salpêtrière, Inserm U1127, CNRS UMR 7225, UPMC UMR S 1127, F-75013, Paris, France. Tel: +33157274651; Fax: +33157274682; Email: olga.corti@upmc.fr.

[#]current address: Laboratoire chémogénétique Servier-Diverchim, Institut du Cerveau et de la Moelle, Paris, France.

[†]The authors wish it to be known that, in their opinion, the first two authors should be regarded as joint First Authors.

Abstract

Mutations in *PARK2*, encoding the E3 ubiquitin protein ligase Parkin, are a common cause of autosomal recessive Parkinson's disease (PD). Loss of *PARK2* function compromises mitochondrial quality by affecting mitochondrial biogenesis, bioenergetics, dynamics, transport and turnover. We investigated the impact of *PARK2* dysfunction on the endoplasmic reticulum (ER)-mitochondria interface, which mediates Ca^{2+} exchange between the two compartments and is essential for Parkin-dependent mitophagy. Confocal and electron microscopy analyses showed the ER and mitochondria to be in closer proximity in primary fibroblasts from *PARK2* KO mice and PD patients with *PARK2* mutations than in controls. Ca^{2+} flux to the cytosol was also modified, due to enhanced ER-to-mitochondria Ca^{2+} transfers, a change that was also observed in neurons derived from induced pluripotent stem cells of a patient with *PARK2* mutations. Subcellular fractionation showed the abundance of the Parkin substrate mitofusin 2 (Mfn2), which is known to modulate the ER-mitochondria interface, to be specifically higher in the mitochondrion-associated ER membrane compartment in *PARK2* KO tissue. Mfn2 downregulation or the exogenous expression of normal Parkin restored cytosolic Ca^{2+} transients in fibroblasts from patients with *PARK2* mutations. By contrast, a catalytically inactive PD-related Parkin variant had no effect. Overall, our data suggest that Parkin is directly involved in regulating ER-mitochondria contacts and provide new insight into the role of the loss of Parkin function in PD development.

Introduction

Parkinson's disease (PD) is a common invalidating movement disorder caused by progressive degeneration of the dopaminergic neurons of the *substantia nigra pars compacta*. Most cases of PD are sporadic, but almost 10% display Mendelian inheritance. Loss of function mutations of the *PARK2* and *PARK6* genes, encoding the cytosolic E3 ubiquitin protein ligase Parkin and the mitochondrial serine/threonine kinase PINK1, account for a large proportion of early-onset autosomal recessive PD cases (1).

Mitochondrial dysfunction has emerged as a key player in autosomal recessive PD (2, 3). Studies in *Drosophila* models have demonstrated that Parkin and PINK1 cooperate in a pathway maintaining mitochondrial function (4-7). These proteins ensure mitochondrial quality by eliminating damaged mitochondria in a process known as mitophagy (8-11), but they have also been reported to regulate mitochondrial calcium (Ca^{2+}) homeostasis (12, 13), mitochondrial dynamics (14-17), bioenergetics (18, 19), biogenesis (20-22), and apoptotic cell death (13, 23). Most, if not all of these functions are mediated by the ER-mitochondria interface, a region of close apposition between the ER and outer mitochondrial (OM) membranes, historically linked to lipid metabolism and Ca^{2+} signaling (24, 25). This interface is enriched in ER Ca^{2+}-releasing receptors (inositol 1,4,5-triphosphate (IP_3) receptors) and mitochondrial Ca^{2+} transporters (voltage-dependent anion channels, VDACs) involved in ER-to-mitochondria Ca^{2+} transfer. It thus plays crucial physiology roles in the maintenance of mitochondrial bioenergetics, buffering of cytotoxic increases in Ca^{2+} concentration and the induction of apoptosis.

A protein complex tethering the ER to mitochondria has been identified in yeast, and several candidates for this role have been identified in mammalian cells (24). Mitofusin 2 (Mfn2), which is present on both the ER and OM membranes, is a well-established modulator of ER-mitochondrial coupling, although its potential role as a tether remains a matter of debate (26-28). Parkin interacts with and ubiquitylates several proteins associated with the ER-mitochondria interface (29), including VDACs and Mfn2, and may itself associate with this interface, particularly in conditions of stress (30). Moreover, Parkin-dependent mitophagy begins in this compartment (31).

We investigated the mechanisms underlying *PARK2*-linked PD, by characterizing the ER-mitochondria interface in primary mouse embryonic fibroblasts (MEFs) from *PARK2* KO mice and

fibroblasts from PD patients with *PARK2* mutations. We found that the loss of *PARK2* function exacerbated ER-mitochondria juxtaposition in these models, leading to aberrant ER-to-mitochondria Ca^{2+} transfers that were corrected by decreasing the abundance of Mfn2 or by producing a functional Parkin protein.

Results

Loss of *PARK2* function brings the ER and mitochondria closer together. In MEFs from wild-type mice and fibroblasts from unaffected individuals, Parkin was detected at the expected apparent molecular mass of 52 kDa (Fig. S1A and 1A). In human fibroblasts, an additional shorter (42 kDa) isoform was observed, probably resulting from the use of an internal translational initiation codon (Fig. 1A, (32)). No signal corresponding to Parkin was observed in *PARK2* KO MEFs or in fibroblasts from six patients with five different compound heterozygous *PARK2* mutations, including single-amino acid substitutions (Table 1).

Confocal live-cell imaging revealed a significantly higher degree of colocalization for the signals corresponding to the exogenously expressed ER marker GFP-Sec61 and the mitochondrial dye tetramethylrhodamine methyl ester (TMRM) in fibroblasts from patients with *PARK2* mutations (28% increase in Mander's overlap coefficient, Fig. 1B) than in control cells. Greater colocalization of the ER and mitochondria, stained with ER-Tracker and MitoTracker dyes, respectively, was also observed in *PARK2* KO MEFs than in wild-type MEFs (Fig. S1B). To overcome the spatial resolution limit of confocal microscopy (circa 200 nm) we assessed the proximity of the ER and mitochondria by using various electron microscopy methods. In fibroblasts from patients with *PARK2* mutations, 14.2% of the area within 500 nm of the mitochondria was occupied by ER tubules, versus only 9.8% in control fibroblasts (Fig. 1C). In addition, in *PARK2* KO MEFs, 32% of the mitochondria were in direct contact with the ER in the observed plane, versus only 22% in wild-type cells (Fig. S1C, *Left*). In this model, *PARK2* deletion was also associated with a decrease of almost 40% in the apparent minimum distance between the surface of the mitochondria and the closest ER tubules (Fig. S1C, *Right*). We found no major differences in mitochondrial size or the proportion of swollen mitochondria linked to the loss of *PARK2* function in these models (Fig. S2). Moreover, there was no correlation between Mander's coefficient values or proportion of area around mitochondria covered by ER and the age of the donors, excluding bias related to age differences at the time of biopsy between patients and control subjects (Fig. S3A and B).

The loss of *PARK2* function disturbs intracellular Ca^{2+} homeostasis. We then investigated whether the smaller distance between the ER and mitochondria affected Ca^{2+} transients in cells with *PARK2*

mutations. Together with ryanodine receptors, IP_3 receptors (IP_3R) are the major route of Ca^{2+} release from the ER, and they are also a key element of contact sites between the ER and mitochondria (33). We compared IP_3R-induced cytosolic Ca^{2+} transients in fibroblasts from *PARK2* patients and KO mice with those in the corresponding controls, using the ratiometric cytosolic Ca^{2+} probe Fura-2. When challenged with bradykinin (BK), which stimulates the production of IP_3 through the B_2 receptor (B_2R)-dependent activation of phospholipase C, IP_3R-mediated cytosolic transients were significantly lower in fibroblasts with *PARK2* mutations than in control cells: the 340/387nm ratio peak was 24% lower in cells from patients (Fig. 2A) and 39% lower in cells from *PARK2* KO mice (Fig. S4A). Again, there was no correlation between Fura-2 fluorescence values and donor age (Fig. S3C). We ruled out an effect of *PARK2* mutations on B_2R function, by challenging Fura-2-loaded cells with ATP or histamine (His), which trigger IP_3 generation by stimulating P2Y or H_1 receptors. Similar results were obtained (Fig. 2B and S4B).

The assessment of all intracellular Ca^{2+} pools with the Ca^{2+} ionophore ionomycin (Iono) revealed no difference in the Fura-2 signal peak between fibroblasts with *PARK2* mutations and controls (Fig. 2C). We also investigated Ca^{2+} storage in the ER and IP_3R-mediated Ca^{2+}-release capacity directly (Fig. 2D). Cells loaded with the low-affinity ratiometric Ca^{2+} indicator Mag-Fura-2 were permeabilized with digitonin to remove the cytosolic probe pool and to unmask the signal of the Ca^{2+}-bound reporter in the ER, the major Ca^{2+} storage organelle. The ER signal was similar in fibroblasts with *PARK2* mutations and in control cells (Fig. 2D, *250s*); moreover, it decayed with similar kinetics following IP_3 challenge (Fig. 2D, *350 s*), suggesting that ER Ca^{2+} concentration and IP_3R function were not affected by *PARK2* mutations.

Using Fura-2, we also compared cytosolic Ca^{2+} transients in induced pluripotent stem cell (iPSC)-derived neurons from control individuals and a patient included in this study (Fig. 2E and F, S5 and S6). Following stimulation with His, the signal peak of the *in vitro* differentiated neurons from Patient 2 (Table 1, p.[Ala291ValfsX8];[Arg42Pro]) was 28% smaller than that of the neurons from a control individual (Table 1, Control 9, p.[Ala291ValfsX8];[=], Fig. 2E), consistent with our observations in fibroblasts. As only a small proportion of the neurons responded to His stimulation, we also depolarized the cells with high K^+, a treatment that triggers Ca^{2+} efflux from the ER by different

mechanisms in neurons, including through IP_3R-mediated stimulation (34-36). Cytosolic Ca^{2+} transients induced by high K^+ were significantly lower in neurons from Patient 2 than in those from control individuals (Table 1, Control 2 and Control 9, Fig. 2F).

Loss of *PARK2* function enhances ER-to-mitochondria Ca^{2+} transfers. We determined whether the decrease in IP_3R-evoked cytosolic Ca^{2+} transients in fibroblasts with *PARK2* mutations (Fig. 2A and B) reflected higher levels of Ca^{2+} uptake by negatively charged mitochondria. When cells were treated with the uncoupler carbonyl cyanide 4-(trifluoromethoxy)phenylhydrazone (FCCP) to dissipate the mitochondrial transmembrane potential required for Ca^{2+} import (37), the increases in cytosolic Ca^{2+} concentration triggered by ATP were similar in cells from patients and controls (Fig. 3A). We then monitored Ca^{2+} transients on the mitochondrial surface and in the mitochondrial matrix, with the OM membrane-targeting, low-affinity YFP-based Ca^{2+} indicator, N33-D1cpv (38), and the intramitochondrial Ca^{2+} reporter pericam-mt (39). We observed no significant increase in the number of Ca^{2+} hotspots at the mitochondrial surface (data not shown), but the ATP-evoked N33-D1cpv signal peak was 62% higher in fibroblasts with *PARK2* mutations than in control fibroblasts, suggesting that the mitochondria in these cells were exposed to higher Ca^{2+} concentrations (Fig. 3B). In addition, the transient signal corresponding to the Ca^{2+}-bound pericam-mt in fibroblasts from patients was more than 100% higher than that in control cells, confirming that mitochondrial Ca^{2+} uptake was increased in these conditions (Fig. 3C). Absence of correlation between pericam-mt signal peak and donor age indicates that these differences are genuine (Fig. S3D).

Rapid Ca^{2+} import into the mitochondrial matrix leads to transient, reversible membrane depolarization (40). Accordingly, when the cells were treated with BK in the presence of thapsigargin (Tg) to prevent ER Ca^{2+} reuptake, the mitochondrial membrane potential assessed with TMRM decreased more rapidly and strongly in cells with *PARK2* mutations than in control cells (Fig. 3D).

Mfn2 downregulation or the exogenous expression of Parkin restores Ca^{2+} transients in cells with *PARK2* mutations. We investigated whether *PARK2* dysfunction altered the abundance or subcellular distribution of the Parkin substrate Mfn2 (41-44). Steady-state Mfn2 levels in total fractions from the fibroblasts of *PARK2* patients or KO mice did not differ from those in the corresponding controls (Fig. 4A, S7A and B). We investigated the abundance of Mfn2 in specific

subcellular fractions, by obtaining preparations enriched in ER, mitochondria, and mitochondria-associated membranes of the ER (MAM), containing ER-mitochondria contact zones, from the livers of WT and *PARK2* KO mice (Fig. S7C) according to a well-established protocol (45). Steady-state Mfn2 levels were 50% higher specifically in the MAM fraction of *PARK2* KO mice than in that of WT mice (Fig. 4A).

The partial depletion of Mfn2 in fibroblasts from Patient 5 (Table 1, p.[Ala138GlyfsX7];[Asn52MetfsX29]) by RNA interference resulted in a 21% increase in BK-evoked cytosolic Ca^{2+} transients (Fig. 4B). This change is of a similar magnitude to the previously reported difference in mean signal between the fibroblasts of patients with *PARK2* mutations and control fibroblasts (Fig. 2A). Exogenous Parkin expression yielded a similar rescue (Fig. 5A). By contrast, expression of the PD-linked Parkin variant carrying the C441R substitution, affecting the RING2 finger and abolishing catalytic activity *in vitro* (46, 47), had no effect (Fig. 5B).

Discussion

It has recently been suggested that modifications of the ER-mitochondria interface may play a key role in neurodegenerative diseases (48-57). We investigated this subcellular compartment for the first time in primary cells from patients with *PARK2* mutations and from *PARK2* KO mice, by both confocal and electron microscopy approaches. The loss of *PARK2* function in these models resulted in greater proximity between the ER and mitochondria than in control cells. In addition, it disrupted cellular Ca^{2+} dynamics, leading to an increase in mitochondrial Ca^{2+} uptake accompanied by a decrease in cytosolic fluxes following ER-mediated Ca^{2+} release (Fig. 6). These effects were also observed in iPSC-derived neurons from a patient with *PARK2* mutations. Exogenous Parkin expression restored cytosolic Ca^{2+} transients to normal levels, suggesting that these defects constitute a primary phenotype related to *PARK2* dysfunction rather than compensatory adaptations.

The alteration of ER-to-mitochondria Ca^{2+} exchanges has been linked to mitochondrial Ca^{2+} overload, mitochondrial permeability transition and programmed cell death (58, 59). The phenotype identified here may thus be a key element of neuronal vulnerability in *PARK2*-linked PD. Sustained exposure to abnormally high Ca^{2+} concentrations may lower the Ca^{2+} buffering capacity of the mitochondria, increasing the likelihood of permeability transition in cells with a dysfunctional *PARK2* gene. This situation has been reported following the artificial tightening of the ER-mitochondria connectivity by a synthetic linker (60). It may also underlie the reported vulnerability of Parkin-deficient cells to excitotoxic challenges or endoplasmic reticulum stress (30, 61, 62), associated with the excessive influx of extracellular Ca^{2+} and the excessive release of Ca^{2+} from the ER, respectively (63, 64). Conversely, the ability of Parkin to modulate the juxtaposition between the ER and mitochondria may contribute to its broad neuroprotective capacity in these models and in other contexts associated with Ca^{2+} dyshomeostasis (30, 61, 62, 65, 66). Mitochondrial Ca^{2+} overload has also been reported in different cell models associated with PINK1 dysfunction (13, 67, 68), suggesting that it may be a general pathogenic mechanism in autosomal recessive PD. Gandhi and colleagues attributed this effect to impairment of the mitochondrial Na^{+}/Ca^{2+} exchanger mediating Ca^{2+} efflux from the mitochondrial matrix (13), but future studies should consider whether changes to the ER-mitochondria interface contribute to the phenotype.

It has been suggested that Parkin regulates crosstalk between the ER and mitochondria (30, 61, 69, 70). Mitochondrial dysfunction and endoplasmic reticulum stress are closely connected and both may be relevant to PD pathogenesis (reviewed in (71, 72)). Both conditions upregulate *PARK2* expression (61, 66, 69, 70). Parkin associates with the mitochondria and ER surfaces (9, 65, 73), and a recent study showed it to be present in the MAM fraction in neurons following glutamate-mediated excitotoxicity (30). We did not detect Parkin immunoreactivity in MAM fractions from mouse liver, possibly reflecting the transient and dynamic interaction of the protein with this compartment. However, our results suggest that Parkin regulates the turnover of a specific pool of Mfn2 located at the ER-mitochondria interface (Fig. 6). Our data also suggest that an increase in the abundance of Mfn2 at this site may be at least partly responsible for the Ca^{2+} dyshomeostasis in cells with *PARK2* mutations. Our observations are consistent with those of a number of previous studies reporting a positive correlation between Mfn2 abundance in the MAM fraction and the proximity of the ER and mitochondria (74, 75), or the functional rescue of Ca^{2+} or lipid dyshomeostasis following the ablation of Mfn2 in cells with an overdeveloped ER-mitochondria interface (48, 76). These findings are consistent with a contribution of Mfn2 to the tethering of the ER to mitochondria, as initially proposed by de Brito and Scorrano (27). Pioneering studies by Area-Gomez and colleagues, in particular, reported enhanced ER-mitochondrial coupling and changes to lipid metabolism that were rescued by Mfn2 depletion in fibroblasts from presenilin KO mice and from patients with familial and sporadic forms of Alzheimer's disease (48).

Despite these observations, recent studies based on the use of EM and confocal colocalization approaches to investigate the ER-mitochondria interface in Mfn2-deficient models have called into question the role of Mfn2 in ER-mitochondria tethering, suggesting instead that this protein may act as a tethering antagonist (26, 28). This discrepancy highlights the intrinsic structural and functional difficulties involved in studies of contact sites between the ER and mitochondria. Changes to the morphological features of the ER and mitochondria triggered by specific treatments or acute genetic manipulations, and technical limitations, such as the resolution limits of classical confocal microscopy approaches, may introduce bias into these analyses. The highly dynamic and multifaceted nature of ER-mitochondria contacts is probably an additional major hurdle. Various protein complexes have

been implicated in the maintenance of these contacts in mammalian cells ((27, 51, 77), reviewed in (24)), and the type of contacts depends on whether the smooth or rough ER tubules are involved (60). Moreover, acute stress has been associated with a smaller distance between the ER and mitochondria and lower levels of ER-to-mitochondria Ca^{2+} transfer (60). Thus, subtle differences in experimental conditions, the use of different cell types and differences in assessment methodology may account for the apparent contradictions in published results. For example, different effects of presenilin mutants have been observed depending on whether cells transiently transfected to overproduce these proteins, or cells from patients or constitutive KO models were studied (48, 57). Similarly, in contrast to our observations, Cali *et al.* previously reported a decrease in crosstalk between the ER and mitochondria associated with weaker mitochondrial Ca^{2+} transients and ATP production following acute siRNA-mediated Parkin depletion in tumor-derived cell lines (55). These authors made similar observations following the downregulation of two additional PD-linked proteins, α-synuclein and DJ-1 (54, 56). The genetic manipulations in all these studies induced profound changes to the mitochondrial network not observed in fibroblasts from *PARK2* KO mice or from patients with *PARK2* mutations (Fig. S2, (78)). The MAM compartment has also been shown to contain α-synuclein and DJ-1, and phospholipid biosynthesis levels have been shown to be low in cells overproducing PD-linked α-synuclein variants, which display weaker colocalization with the MAM fraction (49, 56). Overall, these findings converge to suggest that disturbances of ER-mitochondria contact play a critical role in PD. Additional studies in primary patient-derived cells, ideally using complementary EM analyses and super-resolution microscopy techniques to follow individual ER-mitochondria contact sites and their dynamics, are required to characterize the nature of these perturbations in PD in a reliable manner.

In conclusion, our study provides the first evidence for a structural and functional defect of the ER-mitochondria interface in primary cells with constitutive *PARK2* dysfunction that may be of particular relevance to the dopaminergic neurons of the *substantia nigra pars compacta*, which have been reported to be especially vulnerable to Ca^{2+} dysregulation (79). Future studies should try to clarify the links between this defect and mitochondrial dysfunction, and their relative contributions to dopaminergic neurodegeneration in *PARK2*-related PD.

Materials and Methods

Mammalian expression vectors, siRNAs, cell culture and transfection. The vectors used were: pcDNA3-HA, pcDNA3-HA-*PARK2* (encoding human Parkin), pcDNA3-HA-*PARK2*^{C441R}, pcDNA3.1-GFP-Sec61β (80) , pcDNA3-N33-D1cvp (38), and ratiometric pericam-mt (39). AllStars negative control siRNA (QIAGEN) and Hs_MFN2_5 FlexiTube siRNA (QIAGEN) were used at a final concentration of 125 nM. Human fibroblasts were obtained from skin biopsies from PD patients and age-matched healthy individuals following routine clinical procedures, with previous written informed consent and the approval of the local ethics committee (*Comité de Protection des Personnes "Ile de France"*). Patients were screened for *PARK2* mutations by exon dosage methods and bidirectional Sanger sequencing of the entire coding sequence, with an ABI 3730 automated sequencer, as previously described (81). Human fibroblasts were cultured in Dulbecco's modified Eagle medium supplemented with 10% fetal bovine serum (Gibco), 1% L-glutamine and 1% penicillin-streptomycin. Human fibroblasts were transfected by electroporation with a Neon™ Transfection System (Invitrogen) according to the manufacturer's instructions.

Subcellular fractionation and western blot analyses. MAM, ER, pure mitochondrial (Mp) and crude fractions were isolated from the livers of wild-type and *PARK2* KO mice (24-months old, (82)) by ultracentrifugation, as previously described (45). The quality of the fractionation procedure was evaluated by western blot analysis of each fraction (20 µg) with antibodies against specific markers: mouse monoclonal anti-immunoglobulin heavy chain-binding protein (BiP, BD Transduction Laboratories, 1:1000; ER, MAM), anti-cytochrome *c* (BD Biosciences, 1:500; mitochondria); rabbit polyclonal anti-Erlin2 (Cell Signaling, 1:1000; ER, MAM), anti-long-chain fatty-acid CoA ligase 4 (ASCL4/FACL4, Santa Cruz Biotechnology, 1:200; MAM), anti-Mfn2 (Abcam, 1:1000; mitochondria, MAM), anti-mitochondrial processing peptidase subunit β (PMPCB, ProteinTech, 1:4000; mitochondria), anti-presenilin 2 (PS2, Cell Signaling, 1:1000; MAM). Other antibodies used for western blotting were: mouse monoclonal anti-Parkin (clone PARK8, Millipore, 1:1000) and rabbit polyclonal anti-actin (Abcam, 1:4000).

Confocal microscopy. Human fibroblasts were transiently transfected with Sec61-GFP and stained with 50 nM TMRM. Live-cell confocal laser microscopy was performed on a Leica SP2 AOBS AOTF

confocal microscope equipped with a PlanApo X63 (NA 1.4) numerical aperture objective. Argon (488 nm) and HeNe (543 nm) laser lines were used for excitation. Images were acquired with a 0.5 μM step in the *z*-direction. The images were not further modified after acquisition, and were analyzed plane-by-plane (4-6 planes per cell) with the colocalization plugin included in the Wright Cell Imaging Facility (WCIF) collection of ImageJ. At least 48 cells were analyzed from each of seven patients and seven controls.

Electron microscopy. Cells were grown in uncoated 12-well plastic plates and fixed with 4% paraformaldehyde (PFA)/2.5% glutaraldehyde in 0.1 M PBS. Sections (50 μm) were cut and post-fixed by incubation in 1% osmium tetroxide for 30 minutes, rinsed in PBS, dehydrated in a graded series of ethanol solutions and embedded in Epon. Ultrathin (70 nm) sections were cut, counterstained with conventional techniques and analyzed with a JEOL 1200EX II electron microscope operating at 80 kV. Series of adjacent micrographs were taken for at least 27 cells from each of five controls and five patients, and then stitched together with the stitching function of Photoshop to reconstitute the morphology of the entire cell. We drew round the mitochondria by hand on micrographs extended by 500 nm with the dilate selection function of ImageJ. We drew around any ER material within 500 nm of the mitochondria by hand and estimated the surface area of this material with the selection and analyze tools of ImageJ.

Calcium imaging. We assessed cytosolic Ca^{2+} dynamics, by loading human fibroblasts with 5 μM Fura-2 AM (Fura-2 acetoxymethyl ester, Molecular Probes, Life Technologies) for 45 minutes at 37°C, and cytosolic Ca^{2+} concentrations were followed as the fluorescence excitation ratio at 340 nm and 380 nm after stimulation with 300 nM bradykinin, 100 μM ATP, 10 μM histamine or 1 μM ionomycin. Thapsigargin and KCl were used at final concentrations of 700 nM and 50 mM. FCCP was applied at 5 μM final concentration for 10 min. Imaging was performed on a Nikon Eclipse Ti microscope with the HCImagecell program.

For the assessment of ER Ca^{2+} homeostasis, cells were loaded with 5 μM Mag-Fura2 (Molecular Probes, Life Technologies). They were then treated very briefly with digitonin (10 μM), which permeabilizes the cell membrane only, such that cytosolic Mag-Fura-2 diffuses in the extracellular medium and is washed away, the remnant Mag-Fura-2 signal corresponding to Mag-Fura-2 trapped

within the ER lumen. Thus, digitonin treatment initiated a rapid increase in F340/F380 ratio, which stabilized after washout was complete, with the stabilized ratio reflecting the calcium concentration of the ER. IP_3R-mediated Ca^{2+} release was monitored by direct stimulation with 10 µM IP_3.

We monitored Ca^{2+} dynamics at the surface of mitochondria by transfecting the cells with the N33-D1cpv construct. Two days after transfection, cells were bathed in HBSS containing 1.2 mM Ca^{2+} at room temperature and stimulated by the addition of 100 µM ATP. Ca^{2+} concentration at the surface of the outer membrane were followed as the ratio of fluorescence emission at 480 nm and 530 nm (excitation at 430 nm) on a Till photonics IMIC system. We analyzed both the mean signal for the mitochondrial network and the presence of Ca^{2+} hotspots, as previously described (38). Intramitochondrial Ca^{2+} was monitored with the mitochondrion-targeted pericam (pericam-mt) on a Leica SP2 AOBS ATOF confocal microscope equipped with a PlanApo X63 (NA 1.4) numerical aperture objective. The fluorescence of the probe was monitored only for excitation at 405 nm, because emission due to excitation at this wavelength is sensitive to changes in $[Ca^{2+}]$, whereas emission in response to excitation at 488 nm independently reports changes in pH (83). A large pinhole (set at 2 Airy) was used to prevent bleaching.

Statistical analysis. Statistical analysis was performed with Excel (Microsoft) and Prism 6 (Graph Pad Software). Pooled results are expressed as means ± SEM. Unpaired Student's *t* test was used to analyze statistical significance.

Acknowledgements

We thank S. Forlani (DNA and Cell Bank, Hôpital Pitié-Salpêtrière, Paris, France) for human fibroblast collection and banking and B. Keren (Genetic Department, Hôpital Pitié-Salpêtrière, Paris, France) for iPSC karyotyping. We also thank P. Pizzo, T. Pozzan (University of Padua, Padua, Italy) and R. Tsien (University of California, San Diego, USA) for pN33-D1cvp, G. Voeltz (University of Colorado, Boulder, USA) for GFP-Sec61β and A. Miyawaki (RIKEN Brain Science Institute, Saitama, Japan) for pericam-mt. This work was supported by *Institut national de la santé et de la recherche médicale*, *Fondation de France* (grant Engt 2012 00034508), the *European Union* under the 7th Framework Program (FP7/2007-2013) with grants from MEFOPA (HEALTH-2009-241791), ERA-NET NEURON (REPark) and AETIONOMY (Innovative Medicines Initiative Joint Undertaking under grant agreement n°115568, EFPIA companies' in kind contribution), *Fondation Institut du Cerveau et de la Moelle épinière*, and *Agence Nationale pour la Recherche* ("Investissements d'avenir", grant ANR-10-IAIHU-06). C.A.G. was supported by *Fondation pour la recherché médicale*.

Conflict of Interest statement. None declared.

References

1. Corti, O., Lesage, S. and Brice, A. (2011) What genetics tells us about the causes and mechanisms of Parkinson's disease. *Physiol. Rev.*, **91**, 1161-1218.

2. Exner, N., Lutz, A.K., Haass, C. and Winklhofer, K.F. (2012) Mitochondrial dysfunction in Parkinson's disease: molecular mechanisms and pathophysiological consequences. *EMBO J.*, **31**, 3038-3062.

3. Ryan, B.J., Hoek, S., Fon, E.A. and Wade-Martins, R. (2015) Mitochondrial dysfunction and mitophagy in Parkinson's: from familial to sporadic disease. *Trends Biochem. Sci.*, **40**, 200-210.

4. Greene, J.C., Whitworth, A.J., Kuo, I., Andrews, L.A., Feany, M.B. and Pallanck, L.J. (2003) Mitochondrial pathology and apoptotic muscle degeneration in Drosophila parkin mutants. *Proc. Natl. Acad. Sci. U. S. A.*, **100**, 4078-4083.

5. Clark, I.E., Dodson, M.W., Jiang, C., Cao, J.H., Huh, J.R., Seol, J.H., Yoo, S.J., Hay, B.A. and Guo, M. (2006) Drosophila pink1 is required for mitochondrial function and interacts genetically with parkin. *Nature*, **441**, 1162-1166.

6. Park, J., Lee, S.B., Lee, S., Kim, Y., Song, S., Kim, S., Bae, E., Kim, J., Shong, M., Kim, J.M. *et al.* (2006) Mitochondrial dysfunction in Drosophila PINK1 mutants is complemented by parkin. *Nature*, **441**, 1157-1161.

7. Yang, Y., Gehrke, S., Imai, Y., Huang, Z., Ouyang, Y., Wang, J.W., Yang, L., Beal, M.F., Vogel, H. and Lu, B. (2006) Mitochondrial pathology and muscle and dopaminergic neuron degeneration caused by inactivation of Drosophila Pink1 is rescued by Parkin. *Proc. Natl. Acad. Sci. U. S. A.*, **103**, 10793-10798.

8. Matsuda, N., Sato, S., Shiba, K., Okatsu, K., Saisho, K., Gautier, C.A., Sou, Y.S., Saiki, S., Kawajiri, S., Sato, F. *et al.* (2010) PINK1 stabilized by mitochondrial depolarization recruits Parkin to damaged mitochondria and activates latent Parkin for mitophagy. *J. Cell Biol.*, **189**, 211-221.

9. Narendra, D., Tanaka, A., Suen, D.F. and Youle, R.J. (2008) Parkin is recruited selectively to impaired mitochondria and promotes their autophagy. *J. Cell Biol.*, **183**, 795-803.

10. Narendra, D.P., Jin, S.M., Tanaka, A., Suen, D.F., Gautier, C.A., Shen, J., Cookson, M.R. and Youle, R.J. (2010) PINK1 is selectively stabilized on impaired mitochondria to activate Parkin. *PLoS Biol.*, **8**, e1000298.

11. Geisler, S., Holmstrom, K.M., Skujat, D., Fiesel, F.C., Rothfuss, O.C., Kahle, P.J. and Springer, W. (2010) PINK1/Parkin-mediated mitophagy is dependent on VDAC1 and p62/SQSTM1. *Nat. Cell Biol.*, **12**, 119-131.

12. Heeman, B., Van den Haute, C., Aelvoet, S.A., Valsecchi, F., Rodenburg, R.J., Reumers, V., Debyser, Z., Callewaert, G., Koopman, W.J., Willems, P.H. *et al.* (2011) Depletion of PINK1 affects mitochondrial metabolism, calcium homeostasis and energy maintenance. *J. Cell Sci.*, **124**, 1115-1125.

13. Gandhi, S., Wood-Kaczmar, A., Yao, Z., Plun-Favreau, H., Deas, E., Klupsch, K., Downward, J., Latchman, D.S., Tabrizi, S.J., Wood, N.W. *et al.* (2009) PINK1-associated Parkinson's disease is caused by neuronal vulnerability to calcium-induced cell death. *Mol. Cell*, **33**, 627-638.

14. Mortiboys, H., Thomas, K.J., Koopman, W.J., Klaffke, S., Abou-Sleiman, P., Olpin, S., Wood, N.W., Willems, P.H., Smeitink, J.A., Cookson, M.R. *et al.* (2008) Mitochondrial function and morphology are impaired in parkin-mutant fibroblasts. *Ann. Neurol.*, **64**, 555-565.

15. Yu, W., Sun, Y., Guo, S. and Lu, B. (2011) The PINK1/Parkin pathway regulates mitochondrial dynamics and function in mammalian hippocampal and dopaminergic neurons. *Hum. Mol. Genet.*, **20**, 3227-3240.

16. Liu, S., Sawada, T., Lee, S., Yu, W., Silverio, G., Alapatt, P., Millan, I., Shen, A., Saxton, W., Kanao, T. *et al.* (2012) Parkinson's disease-associated kinase PINK1 regulates Miro protein level and axonal transport of mitochondria. *PLoS Genet*, **8**, e1002537.

17. Wang, X., Winter, D., Ashrafi, G., Schlehe, J., Wong, Y.L., Selkoe, D., Rice, S., Steen, J., LaVoie, M.J. and Schwarz, T.L. (2011) PINK1 and Parkin target Miro for phosphorylation and degradation to arrest mitochondrial motility. *Cell*, **147**, 893-906.

18. Damiano, M., Gautier, C.A., Bulteau, A.L., Ferrando-Miguel, R., Gouarne, C., Paoli, M.G., Pruss, R., Auchere, F., L'Hermitte-Stead, C., Bouillaud, F. *et al.* (2014) Tissue- and cell-specific mitochondrial defect in Parkin-deficient mice. *PLoS One*, **9**, e99898.

19. Vincow, E.S., Merrihew, G., Thomas, R.E., Shulman, N.J., Beyer, R.P., MacCoss, M.J. and Pallanck, L.J. (2013) The PINK1-Parkin pathway promotes both mitophagy and selective respiratory chain turnover in vivo. *Proc. Natl. Acad. Sci. U. S. A.*, **110**, 6400-6405.

20. Pacelli, C., De Rasmo, D., Signorile, A., Grattagliano, I., di Tullio, G., D'Orazio, A., Nico, B., Comi, G.P., Ronchi, D., Ferranini, E. *et al.* (2011) Mitochondrial defect and PGC-1alpha dysfunction in parkin-associated familial Parkinson's disease. *Biochim. Biophys. Acta*, **1812**, 1041-1053.

21. Shin, J.H., Ko, H.S., Kang, H., Lee, Y., Lee, Y.I., Pletinkova, O., Troconso, J.C., Dawson, V.L. and Dawson, T.M. (2011) PARIS (ZNF746) repression of PGC-1alpha contributes to neurodegeneration in Parkinson's disease. *Cell*, **144**, 689-702.

22. Gehrke, S., Wu, Z., Klinkenberg, M., Sun, Y., Auburger, G., Guo, S. and Lu, B. (2015) PINK1 and Parkin control localized translation of respiratory chain component mRNAs on mitochondria outer membrane. *Cell Metab.*, **21**, 95-108.

23. Johnson, B.N., Berger, A.K., Cortese, G.P. and Lavoie, M.J. (2012) The ubiquitin E3 ligase parkin regulates the proapoptotic function of Bax. *Proc. Natl. Acad. Sci. U. S. A.*, **109**, 6283-6288.

24. Helle, S.C., Kanfer, G., Kolar, K., Lang, A., Michel, A.H. and Kornmann, B. (2013) Organization and function of membrane contact sites. *Biochim. Biophys. Acta*, **1833**, 2526-2541.

25. Naon, D. and Scorrano, L. (2014) At the right distance: ER-mitochondria juxtaposition in cell life and death. *Biochim. Biophys. Acta*, **1843**, 2184-2194.

26. Cosson, P., Marchetti, A., Ravazzola, M. and Orci, L. (2012) Mitofusin-2 independent juxtaposition of endoplasmic reticulum and mitochondria: an ultrastructural study. *PLoS One*, **7**, e46293.

27. de Brito, O.M. and Scorrano, L. (2008) Mitofusin 2 tethers endoplasmic reticulum to mitochondria. *Nature*, **456**, 605-610.

28. Filadi, R., Greotti, E., Turacchio, G., Luini, A., Pozzan, T. and Pizzo, P. (2015) Mitofusin 2 ablation increases endoplasmic reticulum-mitochondria coupling. *Proc. Natl. Acad. Sci. U. S. A.*, **112**, E2174-2181.

29. Sarraf, S.A., Raman, M., Guarani-Pereira, V., Sowa, M.E., Huttlin, E.L., Gygi, S.P. and Harper, J.W. (2013) Landscape of the PARKIN-dependent ubiquitylome in response to mitochondrial depolarization. *Nature*, **496**, 372-376.

30. Van Laar, V.S., Roy, N., Liu, A., Rajprohat, S., Arnold, B., Dukes, A.A., Holbein, C.D. and Berman, S.B. (2015) Glutamate excitotoxicity in neurons triggers mitochondrial and endoplasmic reticulum accumulation of Parkin, and, in the presence of N-acetyl cysteine, mitophagy. *Neurobiol. Dis.*, **74**, 180-193.

31. Yang, J.Y. and Yang, W.Y. (2013) Bit-by-bit autophagic removal of parkin-labelled mitochondria. *Nat Commun*, **4**, 2428.

32. Henn, I.H., Gostner, J.M., Lackner, P., Tatzelt, J. and Winklhofer, K.F. (2005) Pathogenic mutations inactivate parkin by distinct mechanisms. *J. Neurochem.*, **92**, 114-122.

33. Rizzuto, R., Pinton, P., Carrington, W., Fay, F.S., Fogarty, K.E., Lifshitz, L.M., Tuft, R.A. and Pozzan, T. (1998) Close contacts with the endoplasmic reticulum as determinants of mitochondrial Ca2+ responses. *Science*, **280**, 1763-1766.

34. Friel, D.D. and Tsien, R.W. (1992) A caffeine- and ryanodine-sensitive Ca2+ store in bullfrog sympathetic neurones modulates effects of Ca2+ entry on [Ca2+]i. *J. Physiol.*, **450**, 217-246.

35. Okubo, Y., Kakizawa, S., Hirose, K. and Iino, M. (2001) Visualization of IP(3) dynamics reveals a novel AMPA receptor-triggered IP(3) production pathway mediated by voltage-dependent Ca(2+) influx in Purkinje cells. *Neuron*, **32**, 113-122.

36. Ryglewski, S., Pflueger, H.J. and Duch, C. (2007) Expanding the neuron's calcium signaling repertoire: intracellular calcium release via voltage-induced PLC and IP3R activation. *PLoS Biol.*, **5**, e66.

37. Kirichok, Y., Krapivinsky, G. and Clapham, D.E. (2004) The mitochondrial calcium uniporter is a highly selective ion channel. *Nature*, **427**, 360-364.

38. Giacomello, M., Drago, I., Bortolozzi, M., Scorzeto, M., Gianelle, A., Pizzo, P. and Pozzan, T. (2010) Ca2+ hot spots on the mitochondrial surface are generated by Ca2+ mobilization from stores, but not by activation of store-operated Ca2+ channels. *Mol. Cell*, **38**, 280-290.

39. Nagai, T., Sawano, A., Park, E.S. and Miyawaki, A. (2001) Circularly permuted green fluorescent proteins engineered to sense Ca2+. *Proc. Natl. Acad. Sci. U. S. A.*, **98**, 3197-3202.

40. Chalmers, S. and McCarron, J.G. (2008) The mitochondrial membrane potential and Ca2+ oscillations in smooth muscle. *J. Cell Sci.*, **121**, 75-85.

41. Gegg, M.E., Cooper, J.M., Chau, K.Y., Rojo, M., Schapira, A.H. and Taanman, J.W. (2010) Mitofusin 1 and mitofusin 2 are ubiquitinated in a PINK1/parkin-dependent manner upon induction of mitophagy. *Hum. Mol. Genet.*, **19**, 4861-4870.

42. Rakovic, A., Grunewald, A., Kottwitz, J., Bruggemann, N., Pramstaller, P.P., Lohmann, K. and Klein, C. (2011) Mutations in PINK1 and Parkin impair ubiquitination of Mitofusins in human fibroblasts. *PLoS One*, **6**, e16746.

43. Tanaka, A., Cleland, M.M., Xu, S., Narendra, D.P., Suen, D.F., Karbowski, M. and Youle, R.J. (2010) Proteasome and p97 mediate mitophagy and degradation of mitofusins induced by Parkin. *J. Cell Biol.*, **191**, 1367-1380.

44. Ziviani, E., Tao, R.N. and Whitworth, A.J. (2010) Drosophila parkin requires PINK1 for mitochondrial translocation and ubiquitinates mitofusin. *Proc. Natl. Acad. Sci. U. S. A.*, **107**, 5018-5023.

45. Wieckowski, M.R., Giorgi, C., Lebiedzinska, M., Duszynski, J. and Pinton, P. (2009) Isolation of mitochondria-associated membranes and mitochondria from animal tissues and cells. *Nat. Protoc.*, **4**, 1582-1590.

46. Hampe, C., Ardila-Osorio, H., Fournier, M., Brice, A. and Corti, O. (2006) Biochemical analysis of Parkinson's disease-causing variants of Parkin, an E3 ubiquitin-protein ligase with monoubiquitylation capacity. *Hum. Mol. Genet.*, **15**, 2059-2075.

47. Matsuda, N., Kitami, T., Suzuki, T., Mizuno, Y., Hattori, N. and Tanaka, K. (2006) Diverse effects of pathogenic mutations of Parkin that catalyze multiple monoubiquitylation in vitro. *J. Biol. Chem.*, **281**, 3204-3209.

48. Area-Gomez, E., Del Carmen Lara Castillo, M., Tambini, M.D., Guardia-Laguarta, C., de Groof, A.J., Madra, M., Ikenouchi, J., Umeda, M., Bird, T.D., Sturley, S.L. *et al.* (2012) Upregulated function of mitochondria-associated ER membranes in Alzheimer disease. *EMBO J.*, **31**, 4106-4123.

49. Guardia-Laguarta, C., Area-Gomez, E., Rub, C., Liu, Y., Magrane, J., Becker, D., Voos, W., Schon, E.A. and Przedborski, S. (2014) alpha-Synuclein is localized to mitochondria-associated ER membranes. *J. Neurosci.*, **34**, 249-259.

50. Sano, R., Annunziata, I., Patterson, A., Moshiach, S., Gomero, E., Opferman, J., Forte, M. and d'Azzo, A. (2009) GM1-ganglioside accumulation at the mitochondria-associated ER membranes links ER stress to Ca(2+)-dependent mitochondrial apoptosis. *Mol. Cell*, **36**, 500-511.

51. Stoica, R., De Vos, K.J., Paillusson, S., Mueller, S., Sancho, R.M., Lau, K.F., Vizcay-Barrena, G., Lin, W.L., Xu, Y.F., Lewis, J. *et al.* (2014) ER-mitochondria associations are regulated by the VAPB-PTPIP51 interaction and are disrupted by ALS/FTD-associated TDP-43. *Nat Commun*, **5**, 3996.

52. Tambini, M.D., Pera, M., Kanter, E., Yang, H., Guardia-Laguarta, C., Holtzman, D., Sulzer, D., Area-Gomez, E. and Schon, E.A. (2016) ApoE4 upregulates the activity of mitochondria-associated ER membranes. *EMBO Rep*, **17**, 27-36.

53. Hedskog, L., Pinho, C.M., Filadi, R., Ronnback, A., Hertwig, L., Wiehager, B., Larssen, P., Gellhaar, S., Sandebring, A., Westerlund, M. *et al.* (2013) Modulation of the endoplasmic reticulum-mitochondria interface in Alzheimer's disease and related models. *Proc. Natl. Acad. Sci. U. S. A.*, **110**, 7916-7921.

54. Cali, T., Ottolini, D., Negro, A. and Brini, M. (2012) alpha-Synuclein controls mitochondrial calcium homeostasis by enhancing endoplasmic reticulum-mitochondria interactions. *J. Biol. Chem.*, **287**, 17914-17929.

55. Cali, T., Ottolini, D., Negro, A. and Brini, M. (2013) Enhanced parkin levels favor ER-mitochondria crosstalk and guarantee Ca(2+) transfer to sustain cell bioenergetics. *Biochim. Biophys. Acta*, **1832**, 495-508.

56. Ottolini, D., Cali, T., Negro, A. and Brini, M. (2013) The Parkinson disease-related protein DJ-1 counteracts mitochondrial impairment induced by the tumour suppressor protein p53 by enhancing endoplasmic reticulum-mitochondria tethering. *Hum. Mol. Genet.*, **22**, 2152-2168.

57. Zampese, E., Fasolato, C., Kipanyula, M.J., Bortolozzi, M., Pozzan, T. and Pizzo, P. (2011) Presenilin 2 modulates endoplasmic reticulum (ER)-mitochondria interactions and Ca2+ cross-talk. *Proc. Natl. Acad. Sci. U. S. A.*, **108**, 2777-2782.

58. Fontaine, E., Eriksson, O., Ichas, F. and Bernardi, P. (1998) Regulation of the permeability transition pore in skeletal muscle mitochondria. Modulation By electron flow through the respiratory chain complex i. *J. Biol. Chem.*, **273**, 12662-12668.

59. Abeti, R. and Abramov, A.Y. (2015) Mitochondrial Ca(2+) in neurodegenerative disorders. *Pharmacol. Res.*, **99**, 377-381.

60. Csordas, G., Renken, C., Varnai, P., Walter, L., Weaver, D., Buttle, K.F., Balla, T., Mannella, C.A. and Hajnoczky, G. (2006) Structural and functional features and significance of the physical linkage between ER and mitochondria. *J. Cell Biol.*, **174**, 915-921.

61. Bouman, L., Schlierf, A., Lutz, A.K., Shan, J., Deinlein, A., Kast, J., Galehdar, Z., Palmisano, V., Patenge, N., Berg, D. *et al.* (2011) Parkin is transcriptionally regulated by ATF4: evidence for an interconnection between mitochondrial stress and ER stress. *Cell Death Differ.*, **18**, 769-782.

62. Staropoli, J.F., McDermott, C., Martinat, C., Schulman, B., Demireva, E. and Abeliovich, A. (2003) Parkin is a component of an SCF-like ubiquitin ligase complex and protects postmitotic neurons from kainate excitotoxicity. *Neuron*, **37**, 735-749.

63. Deniaud, A., Sharaf el dein, O., Maillier, E., Poncet, D., Kroemer, G., Lemaire, C. and Brenner, C. (2008) Endoplasmic reticulum stress induces calcium-dependent permeability transition, mitochondrial outer membrane permeabilization and apoptosis. *Oncogene*, **27**, 285-299.

64. Michaels, R.L. and Rothman, S.M. (1990) Glutamate neurotoxicity in vitro: antagonist pharmacology and intracellular calcium concentrations. *J. Neurosci.*, **10**, 283-292.

65. Darios, F., Corti, O., Lucking, C.B., Hampe, C., Muriel, M.P., Abbas, N., Gu, W.J., Hirsch, E.C., Rooney, T., Ruberg, M. *et al.* (2003) Parkin prevents mitochondrial swelling and cytochrome *c* release in mitochondria-dependent cell death. *Hum. Mol. Genet.*, **12**, 517-526.

66. Imai, Y., Soda, M. and Takahashi, R. (2000) Parkin suppresses unfolded protein stress-induced cell death through its E3 ubiquitin-protein ligase activity. *J. Biol. Chem.*, **275**, 35661-35664.

67. Gautier, C.A., Giaime, E., Caballero, E., Nunez, L., Song, Z., Chan, D., Villalobos, C. and Shen, J. (2012) Regulation of mitochondrial permeability transition pore by PINK1. *Mol. Neurodegener.*, **7**, 22.

68. Marongiu, R., Spencer, B., Crews, L., Adame, A., Patrick, C., Trejo, M., Dallapiccola, B., Valente, E.M. and Masliah, E. (2009) Mutant Pink1 induces mitochondrial dysfunction in a neuronal cell model of Parkinson's disease by disturbing calcium flux. *J. Neurochem.*, **108**, 1561-1574.

69. Kim, J.S., Heo, R.W., Kim, H., Yi, C.O., Shin, H.J., Han, J.W. and Roh, G.S. (2014) Salubrinal, ER stress inhibitor, attenuates kainic acid-induced hippocampal cell death. *J. Neural Transm.*, **121**, 1233-1243.

70. Sun, X., Liu, J., Crary, J.F., Malagelada, C., Sulzer, D., Greene, L.A. and Levy, O.A. (2013) ATF4 protects against neuronal death in cellular Parkinson's disease models by maintaining levels of parkin. *J. Neurosci.*, **33**, 2398-2407.

71. Schapira, A.H. (2008) Mitochondria in the aetiology and pathogenesis of Parkinson's disease. *Lancet Neurol.*, **7**, 97-109.

72. Wang, H.Q. and Takahashi, R. (2007) Expanding insights on the involvement of endoplasmic reticulum stress in Parkinson's disease. *Antioxid Redox Signal*, **9**, 553-561.

73. Imai, Y., Soda, M., Hatakeyama, S., Akagi, T., Hashikawa, T., Nakayama, K.I. and Takahashi, R. (2002) CHIP is associated with Parkin, a gene responsible for familial Parkinson's disease, and enhances its ubiquitin ligase activity. *Mol. Cell*, **10**, 55-67.

74. Arruda, A.P., Pers, B.M., Parlakgul, G., Guney, E., Inouye, K. and Hotamisligil, G.S. (2014) Chronic enrichment of hepatic endoplasmic reticulum-mitochondria contact leads to mitochondrial dysfunction in obesity. *Nat. Med.*, **20**, 1427-1435.

75. Sugiura, A., Nagashima, S., Tokuyama, T., Amo, T., Matsuki, Y., Ishido, S., Kudo, Y., McBride, H.M., Fukuda, T., Matsushita, N. *et al.* (2013) MITOL regulates endoplasmic reticulum-mitochondria contacts via Mitofusin2. *Mol. Cell*, **51**, 20-34.

76. Morales, P.E., Torres, G., Sotomayor-Flores, C., Pena-Oyarzun, D., Rivera-Mejias, P., Paredes, F. and Chiong, M. (2014) GLP-1 promotes mitochondrial metabolism in vascular smooth

muscle cells by enhancing endoplasmic reticulum-mitochondria coupling. *Biochem. Biophys. Res. Commun.*, **446**, 410-416.

77. Szabadkai, G., Bianchi, K., Varnai, P., De Stefani, D., Wieckowski, M.R., Cavagna, D., Nagy, A.I., Balla, T. and Rizzuto, R. (2006) Chaperone-mediated coupling of endoplasmic reticulum and mitochondrial Ca2+ channels. *J. Cell Biol.*, **175**, 901-911.

78. Laforge, M., Rodrigues, V., Silvestre, R., Gautier, C., Weil, R., Corti, O. and Estaquier, J. (2016) NF-kappaB pathway controls mitochondrial dynamics. *Cell Death Differ.*, **23**, 89-98.

79. Surmeier, D.J., Guzman, J.N. and Sanchez-Padilla, J. (2010) Calcium, cellular aging, and selective neuronal vulnerability in Parkinson's disease. *Cell Calcium*, **47**, 175-182.

80. Voeltz, G.K., Prinz, W.A., Shibata, Y., Rist, J.M. and Rapoport, T.A. (2006) A class of membrane proteins shaping the tubular endoplasmic reticulum. *Cell*, **124**, 573-586.

81. Periquet, M., Latouche, M., Lohmann, E., Rawal, N., De Michele, G., Ricard, S., Teive, H., Fraix, V., Vidailhet, M., Nicholl, D. *et al.* (2003) Parkin mutations are frequent in patients with isolated early-onset parkinsonism. *Brain*, **126**, 1271-1278.

82. Itier, J.M., Ibanez, P., Mena, M.A., Abbas, N., Cohen-Salmon, C., Bohme, G.A., Laville, M., Pratt, J., Corti, O., Pradier, L. *et al.* (2003) Parkin gene inactivation alters behaviour and dopamine neurotransmission in the mouse. *Hum. Mol. Genet.*, **12**, 2277-2291.

83. Jiang, D., Zhao, L. and Clapham, D.E. (2009) Genome-wide RNAi screen identifies Letm1 as a mitochondrial Ca2+/H+ antiporter. *Science*, **326**, 144-147.

Legends to Figures

Figure 1. Greater ER-mitochondria juxtaposition in fibroblasts with *PARK2* mutations. A. Total extracts from control (Controls 2-4) and *PARK2* (Patients 1-3 and 5-7) fibroblasts were analyzed by western blotting with an anti-Parkin antibody. The arrow indicates the shorter Parkin isoform. Actin served as a loading control. **B.** The colocalization of GFP-Sec61 and TMRM, expressed as mean Mander's overlap coefficient, was analyzed by live confocal microscopy in control (Controls 1-5, 7 and 8) and *PARK2* (Patients 1-7) fibroblasts. **C.** The mean surface area of the ER (green) within 500 nm (purple) of the mitochondria (black) was measured on electron micrographs of control (Controls 1, 2, 5, 7 and 8) and *PARK2* (Patients 2 and 4-7) fibroblasts, and is expressed as a percentage of the total area. Scale bars: 10 μm. *n* represents the number of different fibroblast lines. Error bars indicate the SEM. **p*<0.05.

Figure 2. Disturbed intracellular Ca^{2+} homeostasis in fibroblasts with *PARK2* mutations. A. Monitoring of the Fura-2 340/387 nm signal ratio in control (Controls 1, 2, 4, 5, 7 and 8) and *PARK2* (Patients 2-7) fibroblasts before and after stimulation with BK (*Left*). The BK-induced Fura-2 signal peak was calculated for each cell by subtracting the 340/387 nm ratio at t_0 from the maximal ratio (*Right*). **B.** As in (A) after stimulation with ATP in the absence of extracellular Ca^{2+} and in the presence of Tg. **C.** As in (A) after challenging with ionomycin. **D.** Monitoring of the Mag-Fura-2 340/387 nm signal ratio in control (Controls 1, 2, 4, 5, 7 and 8) and *PARK2* (Patients 1-5 and 7) fibroblasts in basal conditions (0-100 s), after permeabilization with 10 μM digitonin (Dig) in the intracellular medium (100 s), stimulation with 10 μM IP_3 (250 s) and dissipation of Ca^{2+} gradients with ionomycin (375 s, *Left*). The Mag-Fura-2 signal peak corresponds to the mean maximal ratio (*Right*). *n* represents the number of different fibroblast lines . **E.** The His-induced Fura-2 signal peak of Control 9- and Patient 2-derived neurons was measured by subtracting the 340/387 nm ratio at t_0 from the maximal ratio. *n* = 12 cells per IPSC clone from two independent experiments. **F.** The K^+-induced Fura-2 signal peak of Control 2- and Patient 2-derived neurons (*Left*) and of Control 9- and Patient 2-derived neurons (*Right*) was measured by subtracting the 340/387 nm ratio at t_0 from the maximal ratio. *n* = 10 cells per IPSC clone from one of two independent experiments. Error bars represent the SEM. ^{a}p=0.052, **p*<0.05, ***p*<0.01.

Figure 3. Greater ER-to-mitochondria Ca^{2+} transfer in fibroblasts with *PARK2* mutations. A. Monitoring of the Fura-2 signal ratio in control (Controls 1, 2 and 4-7) and *PARK2* (Patients 2-7) fibroblasts, as in (2B), after treatment of the cells with FCCP. **B.** Monitoring of the N33-D1cpv 540/480 nm signal ratio in control (Controls 1-7) and *PARK2* (Patients 1 and 3-7) fibroblasts before and after stimulation with ATP. Due to the high level of variability, the responses for each cell are expressed as the ratio of the signal at a given time point and the mean of the signals before stimulation. **C.** Monitoring of the increase in the pericam-mt 405 nm signal in control (Controls 1, 2, 4, 5 and 7) and *PARK2* (Patients 1-3, 5 and 6) fibroblasts after the addition of ATP. F corresponds to the signal at a given time point and F_0 at t_0. Scale bar: 10 µM. **D.** Monitoring of the TMRM signal in control (Controls 1, 2, 5, 7 and 8) and *PARK2* (Patients 1 and 3-7) fibroblasts before and after simultaneous treatment with Tg and BK. Values represent the % I/I_0, where I is the signal intensity at any time point and I_0 is the signal intensity at t_0. *n* represents the number of different fibroblast lines. Error bars represent the SEM.

Figure 4. Restoration of cytosolic Ca^{2+} transients in fibroblasts with *PARK2* mutations by the partial downregulation of Mfn2. A. Crude, ER, mitochondrial and MAM fractions isolated from the liver of wild-type or *PARK2* KO mice were analyzed by western blotting for Mfn2. Actin, immunoglobulin heavy chain-binding protein (BiP), mitochondrial processing peptidase subunit β (PMPCB) and presenilin 2 (PS2) were used to normalize Mfn2 levels in the crude, ER, mitochondrial and MAM fractions. *n* represents the number of animals for each genotype from three independent experiments. **p*<0.05 (one-tailed *t* test). **B.** Monitoring of the Fura-2 signal ratio before and after stimulation with BK in fibroblasts from Patient 5 transfected with scr siRNA or *MFN2* siRNA. The diagram represents the mean ratio peak from 3 independent experiments in which 85 cells per condition were analyzed (*Right*). Mfn2 levels in the total extracts were monitored by western blotting with normalization against actin (*Left*). *****p*<0.0001. Error bars represent the SEM.

Figure 5. Restoration of cytosolic Ca^{2+} transients in fibroblasts with *PARK2* mutations by Parkin overexpression. A. Monitoring of the Fura-2 signal ratio before and after stimulation with BK in fibroblasts from Patient 5 transfected with pcDNA3-HA (vector) or pcDNA3-HA-*PARK2* (*PARK2*). Parkin expression was verified with an anti-Parkin antibody, using actin as the loading control (*Left*).

The diagram represents the mean ratio peak from 3 independent experiments in which 85 cells per condition were analyzed (*Right*). **B.** As in (A) after the transfection of fibroblasts from Patient 5 with pcDNA3-HA (vector) or pcDNA3-HA-*PARK2*^{C441R} (*PARK2*^{C441R}). ****p<0.0001, *ns* indicates that the difference between the two samples is not significant (*t* test). Error bars represent the SEM.

Figure 6. Model illustrating changes to ER-mitochondria interface and Ca^{2+} transfers in cells with dysfunctional Parkin. Under physiological conditions, Parkin promotes the proteasome-dependent turnover of Mfn2 specifically at the ER-mitochondria interface (*Left*). Parkin dysfunction stabilizes Mfn2 at contact sites, increases ER-mitochondria proximity and IP_3R-dependent ER-mitochondria Ca^{2+} transfers, and decreases cytosolic Ca^{2+} transients (*Right*).

Table 1. Age, sex and genotype of the donors of the skin fibroblasts used in this study.

	Age	**Sex**	***PARK2***	**Parkin**
Control 1	56	F	no mutation	wild-type
Control 2	53	M	no mutation	wild-type
Control 3	65	F	no mutation	wild-type
Control 4	64	F	no mutation	wild-type
Control 5	52	M	no mutation	wild-type
Control 6	61	F	no mutation	wild-type
Control 7	54	M	no mutation	wild-type
Control 8	64	F	no mutation	wild-type
Control 9‡	38	M	c.[(871+1_872-1)_(1083+1_1084-1)del; [=]	p.[Ala291ValfsX8];[=]
Patient 1	65	M	c.[(7+1_8-1)_(171+1_172-1)del]; [101_102delAG]	p.[Val3GlufsX3];[Gln34ArgfsX5]
Patient 2	46	F	c.[(871+1_872-1)_(1083+1_1084-1)del]; [125G>C]	p.[Ala291ValfsX8];[Arg42Pro]
Patient 3	51	F	c.[(871+1_872-1)_(1083+1_1084-1)del]; [125G>C]	p.[Ala291ValfsX8];[Arg42Pro]
Patient 4	40	F	c.[(871+1_872-1)_(1083+1_1084-1)del]; [125G>C]	p.[Ala291ValfsX8];[Arg42Pro]
Patient 5	45	F	c.[(412+1_413-1)_(534+1_535-1)del]; [155delA]	p.[Ala138GlyfsX7];[Asn52MetfsX29]
Patient 6	37	F	c.[(171+1_172-1)_(734+1_735-1)del]; [171+1_172-1)_(534+1_535-1)del]	p.[Asn58GlufsX29];[Asn58_Gln178del]
Patient 7	50	M	c.[(534+1_535-1)_(618+1_619-1)del]; [1321T>C]	p.[Gly179_Ala206del];[Cys441Arg]

‡This control was used exclusively in the experiments involving iPSC-derived neurons.

Abbreviations

Bradykinin, BK; calcium, Ca^{2+}; carbonyl cyanide 4-(trifluoromethoxy)phenylhydrazone, FCCP; endoplasmic reticulum, ER; induced pluripotent stem cell, iPSC; inositol 1,4,5-triphosphate receptors, IP_3R; mitochondria-associated membranes, MAM; mitofusin 2, Mfn2; outer mitochondrial membrane, OM membrane; Parkinson's disease, PD; tetramethylrhodamine methyl ester, TMRM; voltage-dependent anion channels, VDACs

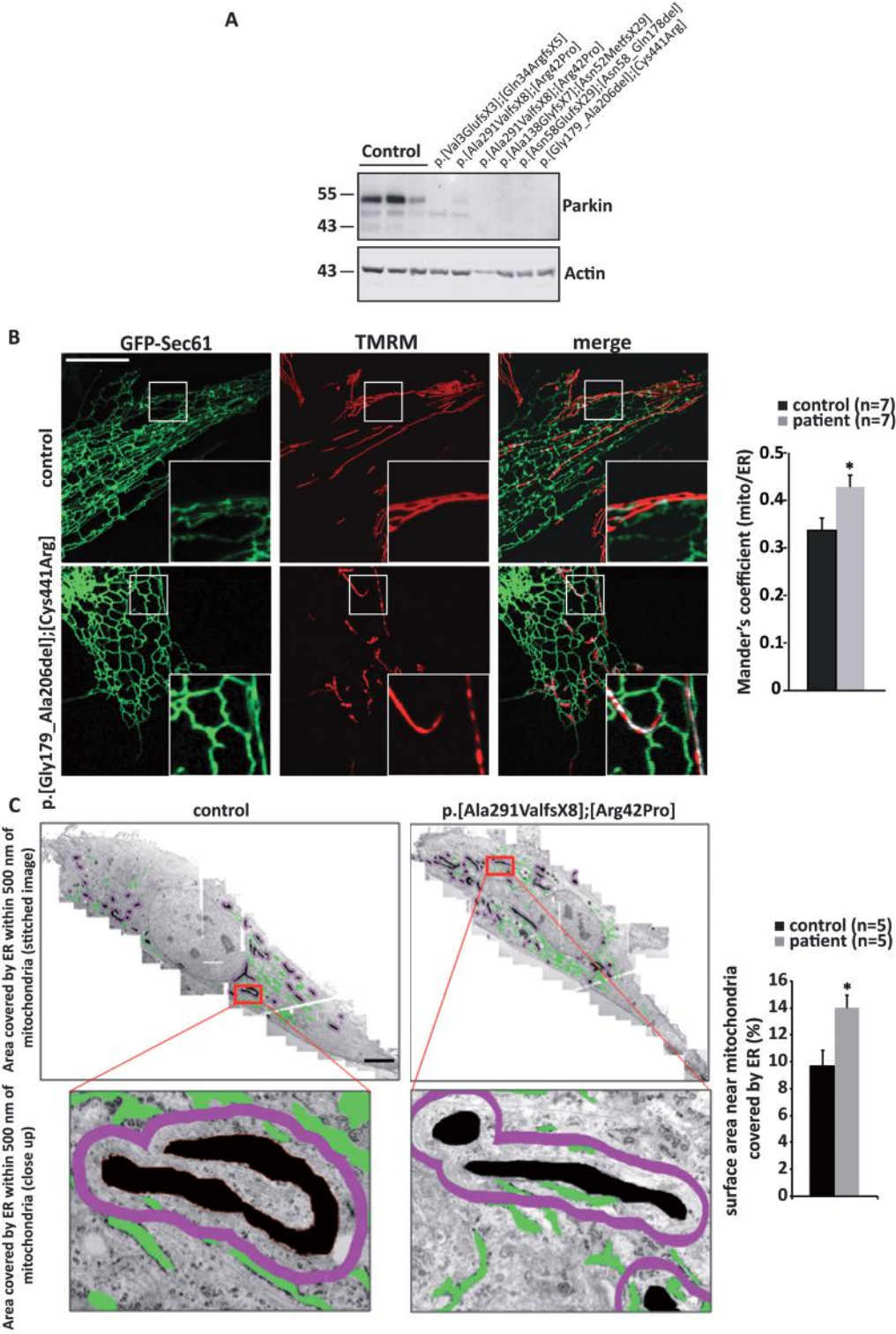
A
Control
p.[Val3GlufsX3];[Gln34ArgfsX5]
p.[Ala291ValfsX8];[Arg42Pro]
p.[Ala291ValfsX8];[Arg42Pro]
p.[Ala138GlyfsX7];[Asn52MetfsX29]
p.[Asn58GlufsX29];[Asn58_Gln178del]
p.[Gly179_Ala206del];[Cys441Arg]
55
43
Parkin
43
Actin
B
GFP-Sec61
TMRM
merge
control
p.[Gly179_Ala206del];[Cys441Arg]
control (n=7)
patient (n=7)
Mander's coefficient (mito/ER)
0.5
0.4
0.3
0.2
0.1
0
*
C
control
p.[Ala291ValfsX8];[Arg42Pro]
Area covered by ER within 500 nm of mitochondria (stitched image)
Area covered by ER within 500 nm of mitochondria (close up)
control (n=5)
patient (n=5)
surface area near mitochondria covered by ER (%)
16
14
12
10
8
6
4
2
0
*

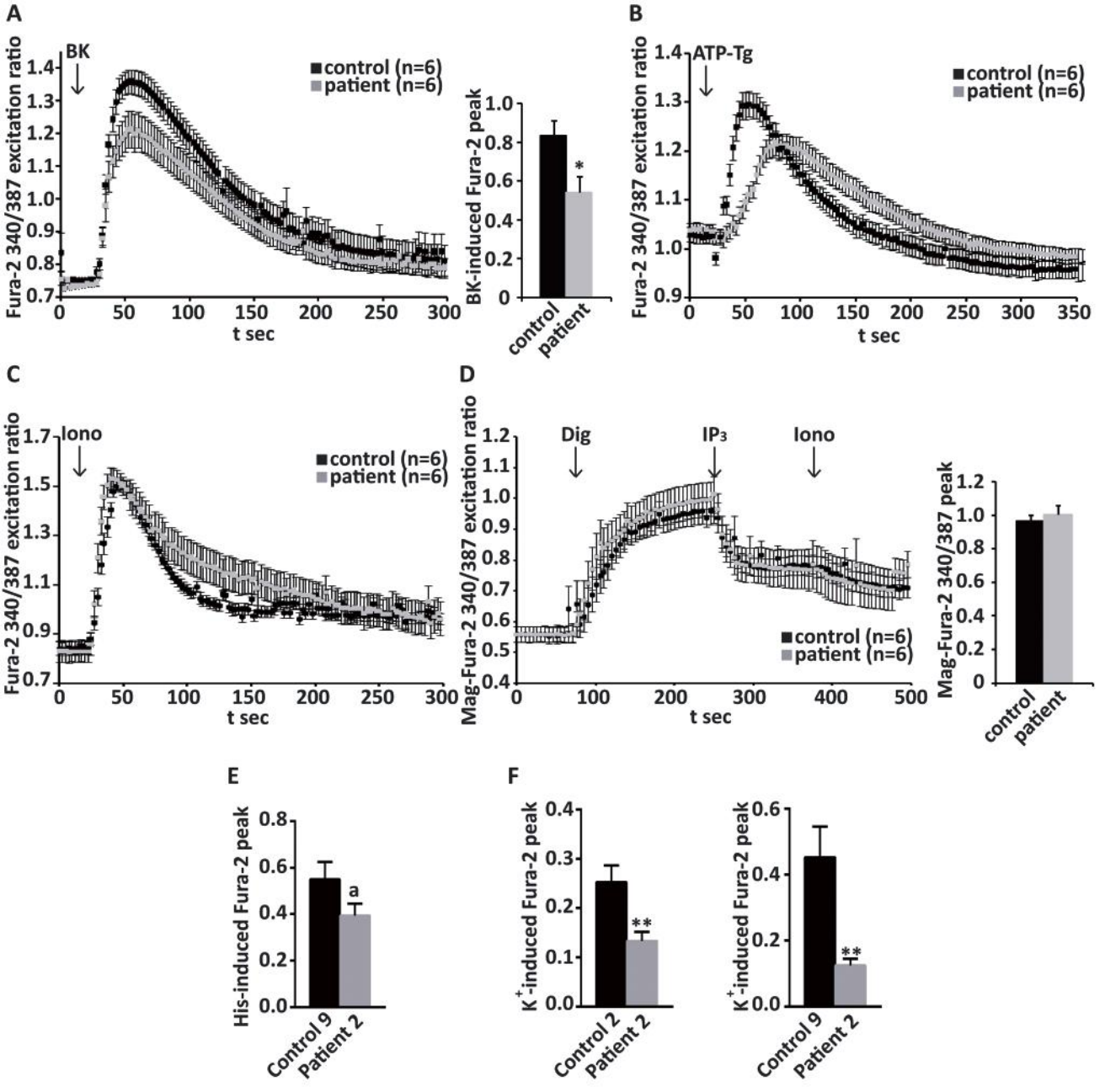
A
BK
control (n=6)
patient (n=6)
Fura-2 340/387 excitation ratio
t sec
BK-induced Fura-2 peak
control
patient
B
ATP-Tg
control (n=6)
patient (n=6)
Fura-2 340/387 excitation ratio
t sec
C
Iono
control (n=6)
patient (n=6)
Fura-2 340/387 excitation ratio
t sec
D
Dig
IP3
Iono
control (n=6)
patient (n=6)
Mag-Fura-2 340/387 excitation ratio
t sec
Mag-Fura-2 340/387 peak
control
patient
E
His-induced Fura-2 peak
a
Control 9
Patient 2
F
K+-induced Fura-2 peak
Control 2
Patient 2
K+-induced Fura-2 peak
Control 9
Patient 2

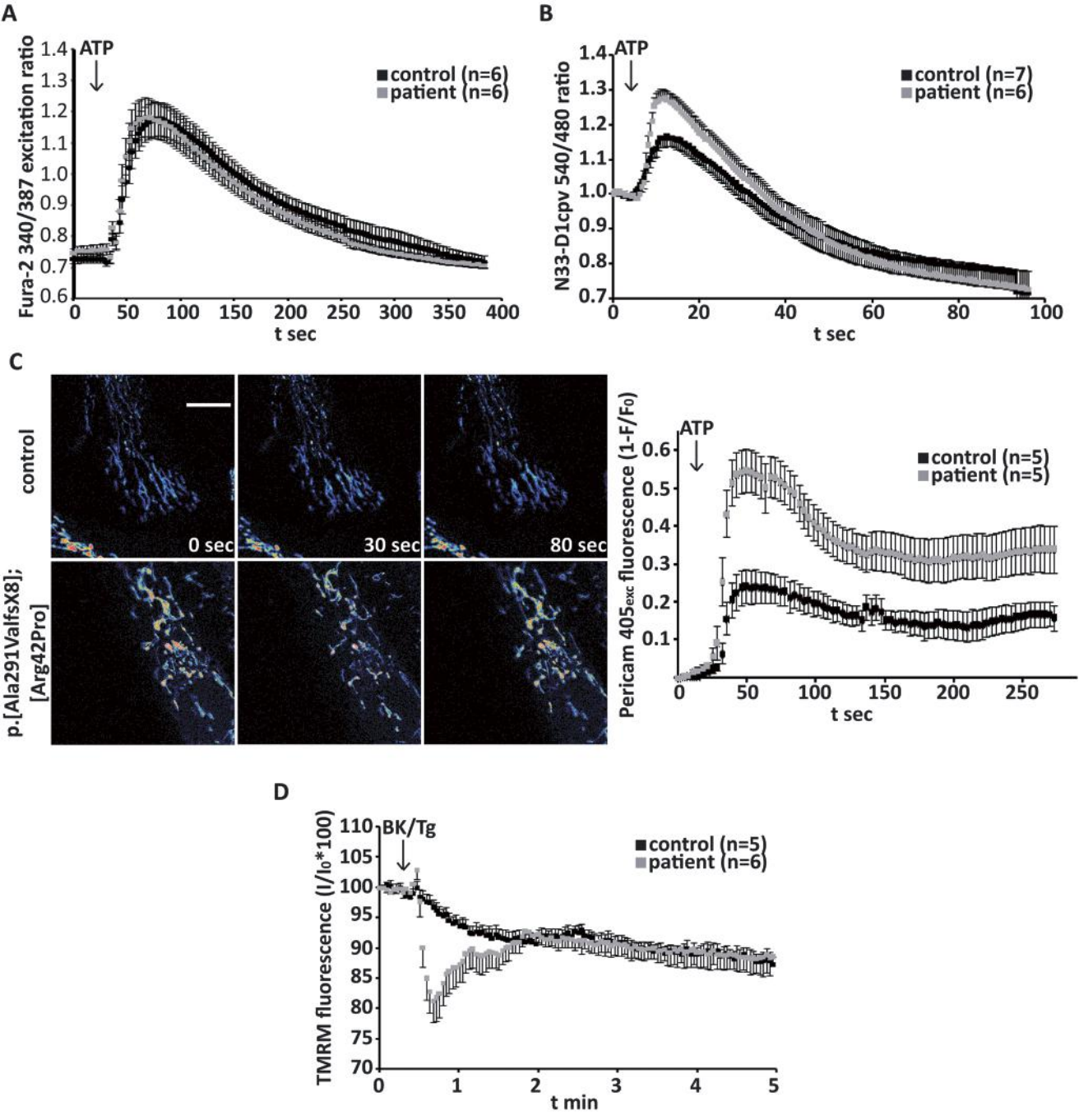
A
ATP
control (n=6)
patient (n=6)
Fura-2 340/387 excitation ratio
t sec
B
ATP
control (n=7)
patient (n=6)
N33-D1cpv 540/480 ratio
t sec
C
control
p.[Ala291ValfsX8];
[Arg42Pro]
0 sec
30 sec
80 sec
ATP
control (n=5)
patient (n=5)
Pericam 405exc fluorescence (1-F/F0)
t sec
D
BK/Tg
control (n=5)
patient (n=6)
TMRM fluorescence (I/I0*100)
t min

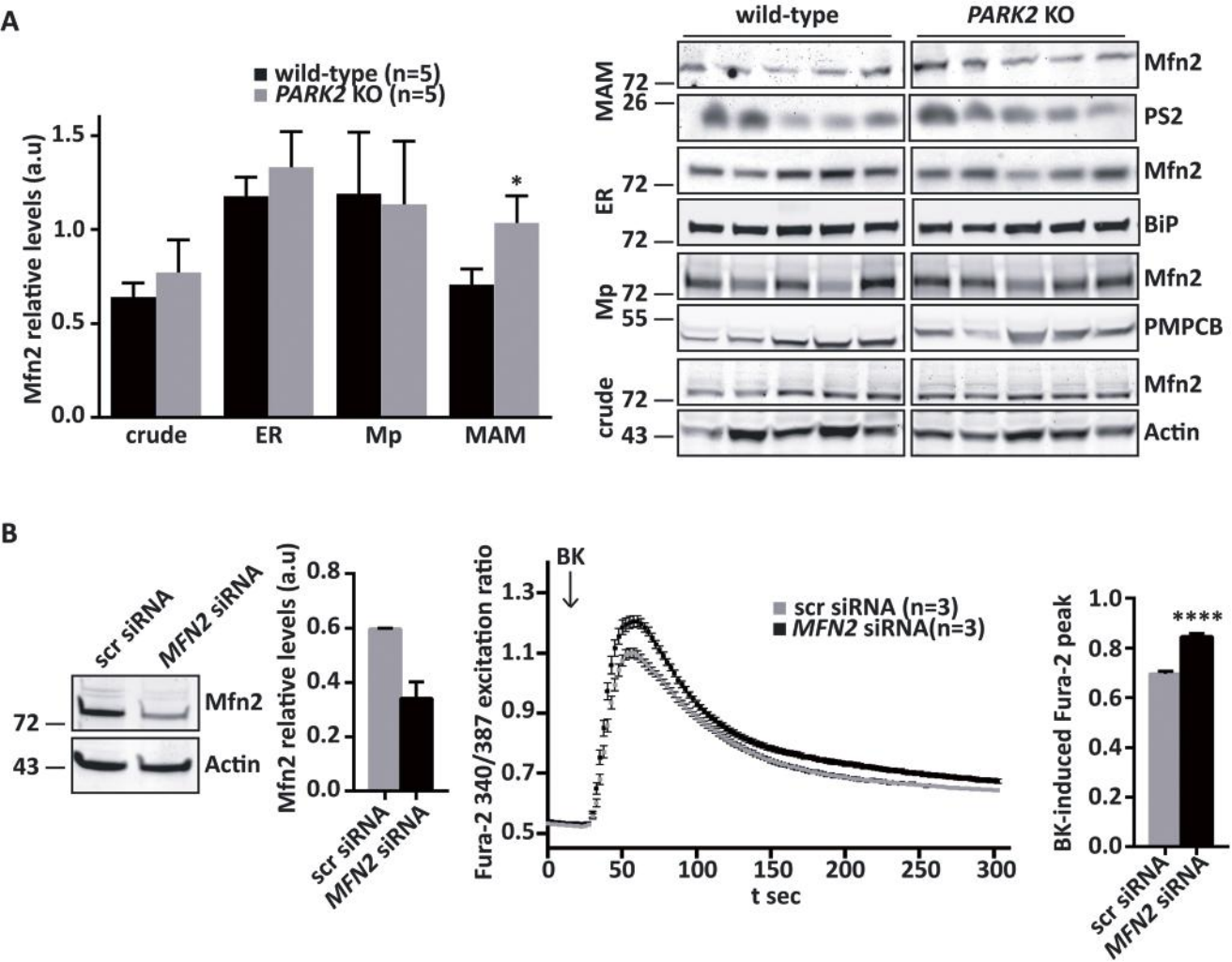
A
wild-type (n=5)
PARK2 KO (n=5)
Mfn2 relative levels (a.u)
1.5
1.0
0.5
0.0
crude
ER
Mp
MAM
*
wild-type
PARK2 KO
MAM
72
26
Mfn2
PS2
ER
72
72
Mfn2
BiP
Mp
72
55
Mfn2
PMPCB
crude
72
43
Mfn2
Actin
B
scr siRNA
MFN2 siRNA
72
43
Mfn2
Actin
Mfn2 relative levels (a.u)
0.8
0.6
0.4
0.2
0.0
scr siRNA
MFN2 siRNA
BK
Fura-2 340/387 excitation ratio
1.3
1.1
0.9
0.7
0.5
scr siRNA (n=3)
MFN2 siRNA(n=3)
0
50
100
150
200
250
300
t sec
BK-induced Fura-2 peak
1.0
0.8
0.6
0.4
0.2
0.0
****
scr siRNA
MFN2 siRNA

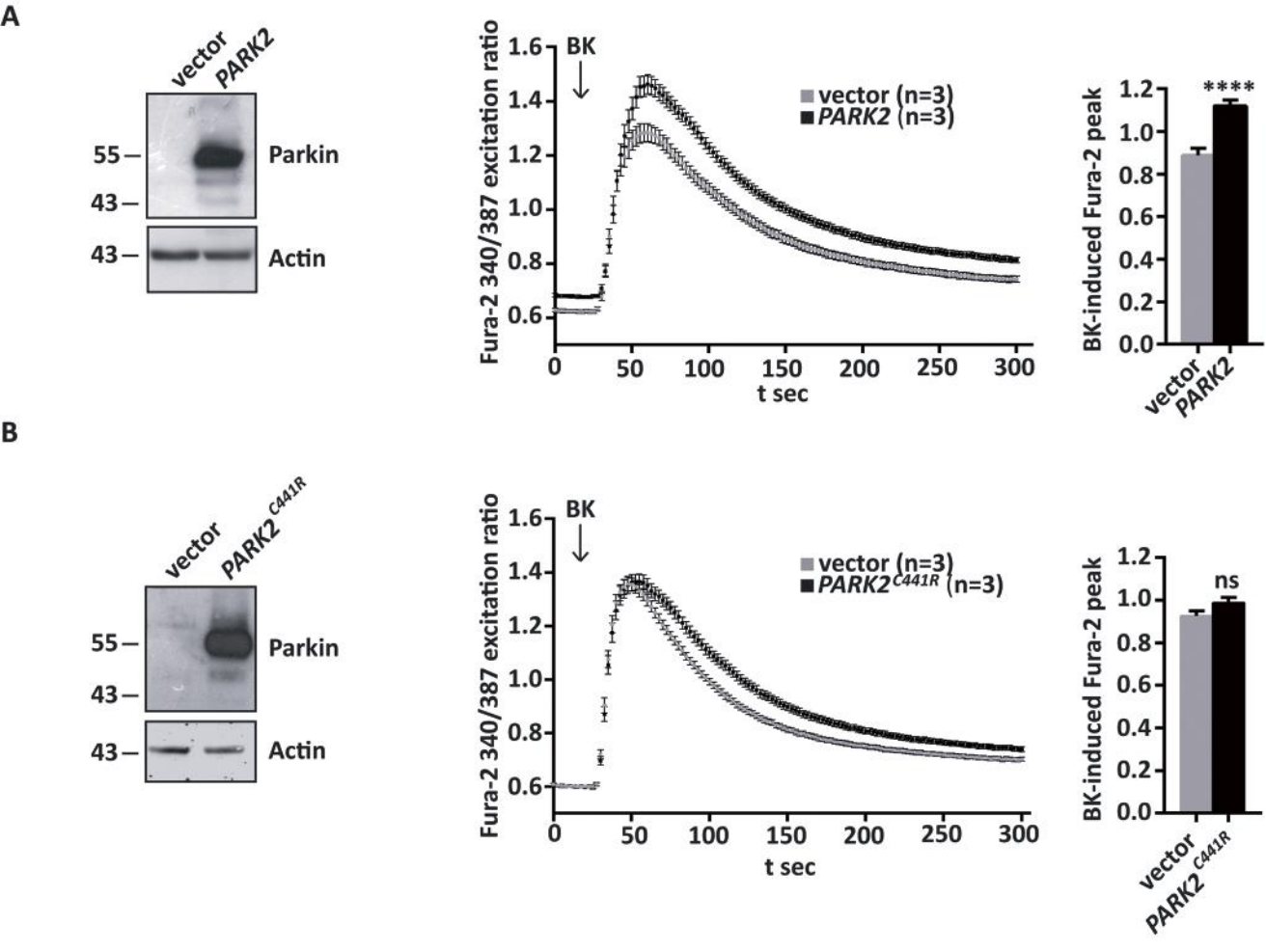
A
vector
PARK2
55
43
Parkin
43
Actin
BK
vector (n=3)
PARK2 (n=3)
Fura-2 340/387 excitation ratio
t sec
BK-induced Fura-2 peak
****
vector
PARK2
B
vector
PARK2C441R
55
43
Parkin
43
Actin
BK
vector (n=3)
PARK2C441R (n=3)
Fura-2 340/387 excitation ratio
t sec
BK-induced Fura-2 peak
ns
vector
PARK2C441R

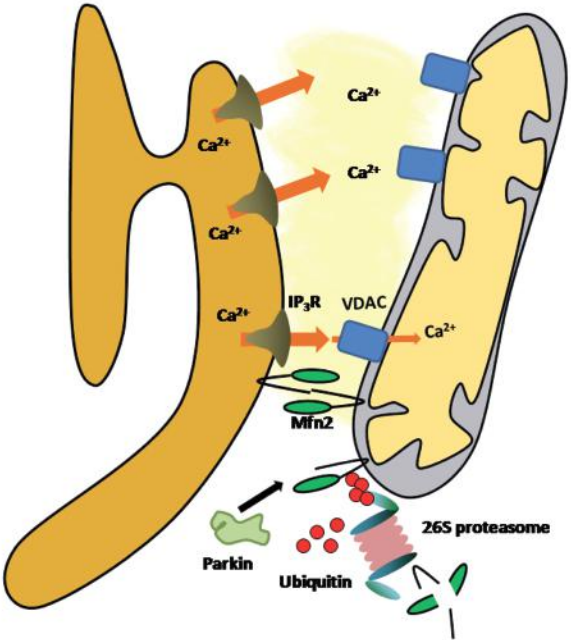

Parkin function

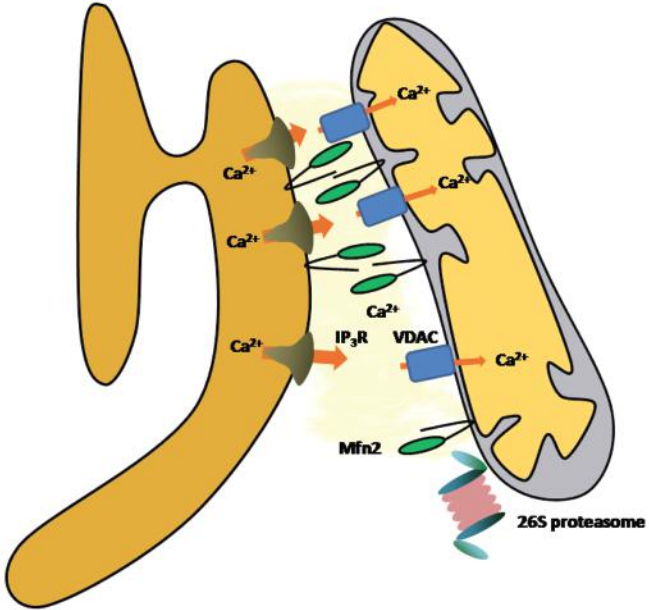

Parkin dysfunction